The effect of shear stress reduction on endothelial cells: a microfluidic study of the actin cytoskeleton

Mehdi Inglebert, Laura Locatelli, Daria Tsvirkun, Jeanette A Maier, Chaouqi Misbah, Lionel Bureau

The effect of shear stress reduction on endothelial cells: a microfluidic study of the actin cytoskeleton

Mehdi Inglebert,[1] Laura Locatelli,[2] Daria Tsvirkun,[1] Jeanette A. Maier,[2] Chaouqi Misbah,[1] and Lionel Bureau[1, a)]
[1)] *Univ. Grenoble Alpes, CNRS, LIPhy, 38000 Grenoble, France*
[2)] *Univ Milan, Dept Biomed & Clin Sci Luigi Sacco, I-20157 Milan, Italy*

(Dated: 3 April 2020)

Reduced blood flow, as occurring in ischemia or resulting from exposure to microgravity such as encountered in space flights, induces a decrease in the level of shear stress sensed by the endothelial cells forming the inner part of blood vessels. In the present study, we use a microvasculature-on-a-chip device in order to investigate *in vitro* the effect of such a reduction in shear stress on shear-adapted endothelial cells. We find that, within one hour of exposition to reduced wall shear stress, human umbilical vein endothelial cells undergo a reorganization of their actin skeleton, with a decrease in the number of stress fibers and actin being recruited into the cells' peripheral band, indicating a fairly fast change in cells' phenotype due to altered flow.

I. INTRODUCTION

The vascular endothelium is the monolayer of specialized cells that lines the inner surface of blood vessels. It is essential to maintaining blood and vascular homeostasis through its functions in biochemical signaling, in vasomotion, and as a selective barrier controlling transport across and interactions with the vessel walls[1,2]. Being in direct contact with blood flow, Endothelial Cells (EC) have been shown to adapt to the hemodynamic forces to which they are exposed[1–3]. One of the first observations of EC adaptation to shear forces produced by blood stream is their elongation and preferred orientation along the flow direction[4]. The establishment of this so-called atheroprotective phenotype[5] involves multiple players. The glycocalyx, or endothelial surface layer (ESL), is the primary structure exposed to blood flow[6–9]. This polymer-rich hydrated layer attached to the apical surface of EC acts, along with others[10–12], as a sensor that transmits, through transmembrane proteins, the mechanical stimulus to the actin cytoskeleton of the cells[8,13]. This triggers a reorganization of the actin network, associated with a remodeling of intercellular junctions and focal adhesions at the basal side of EC[2,8,14,15]. A salient feature of the cytoskeleton of shear-adapted EC is the presence of so-called stress fibers composed of body-spanning elongated bundles of filamentous actin, aligned in the flow direction and contributing to the overall shape and stability of the atheroprotective phenotype[15–17].

While pioneer *in-* or *ex vivo* studies[18–20] have set the basis of the above picture, most of the current knowledge in the field comes from *in vitro* experiments performed using *e.g.* parallel plate flow chambers in which confluent cultured cells are submitted to well-controlled hydrodynamic forces[1]. Recently, microfluidic tools have been combined with EC culture in order to investigate the cellular response to flow in microvessel-mimicking devices[21–23]. It is noteworthy that most *in vitro* studies have been focused on comparing phenotypes or cell organization or signaling between "static" (no flow) and steady-state flow conditions. Only a limited number of works have addressed the question of the response of already shear-adapted EC to a loss of shear stress stimulation[24–27], as would occur for instance in occlusive microvascular events, or as a result of altered hemodynamics such as encountered in space flights[28,29] or in ground simulations of microgravity conditions[30]. To the best of our knowledge, no data have been reported *in vitro* regarding structural changes in the actin cytoskeleton of EC in response to a loss of shear stress stimulation.

In the present work we look at the impact of partial degradation of the ESL and of a 5-fold decrease of shear stress on the actin network reorganization. We do so by using a microvasculature-on-a-chip where endothelial cells are grown to confluence in a network of microchannels[31]. We observe that, when cultured during several days under constant shear stress, endothelial cells elongate in the flow direction and form long and thick stress fibers. A decrease in shear stress results, within one hour, in a disorganization of the stress fibers, combined with an increase in peripheral actin and a thickening of cells' body.

II. MATERIALS AND METHODS

A. Microfluidics

Microchannel networks displaying a diverging/converging geometry (see Fig. 1A) were fabricated using a standard soft lithography technique. A master mold of the network was obtained from a positive photoresist (SU8) cast onto a silicon wafer and exposed to UV light through a quartz-chromium photomask. PDMS (Sylgard 184) was cast onto the mold and cured for 2 hours at 65°C. A glass coverslip (#0, thickness $\approx$100 μm) was used as the bottom part of the microchip and was permanently sealed to the PDMS upper part after exposure of the surfaces of both elements to an oxygen plasma. The thickness of the photoresist on the

[a)] Electronic mail: lionel.bureau@univ-grenoble-alpes.fr

master mold was set such that the series of 16 parallel microchannels in the central part of the network had a square cross-section of 30×30 μm^2. The circuit was connected with silicone tubings to a fluid reservoir at the inlet, and at the outlet to a 1 mL syringe installed on a high precision syringe pump (KDS Legato 110) used in withdraw mode at imposed flow rate.

B. Cell culture and staining

Single donor Human Umbilical Vein Endothelial Cells (HUVEC) were obtained from Promocell GmbH (Germany) and cultured in endothelial cells growth medium supplemented by growth factor (Supplement Mix, Promocell GmbH, Germany).

Before cell seeding, microchannels were activated by exposure to an oxygen plasma (PDC-32G-2 230V, HarrickPlasma, Ithaca, USA) and coated with human fibronectin (50 μg/mL, Cornig) for 30 min at 37 °C. Endothelial cells were suspended in culture medium at a concentration of 10^7 cells/mL and filtered through a nylon cell strainer with pore diameter of 40 μm. The cell suspension was injected into the microchannel network with a pressure controller (OB-1 MK2, Elveflow, France). Consecutive steps of injection of a few seconds and sedimentation periods of several minutes were performed until about 50 % of the network surface was covered by cells.

Cells were then cultured at 37 °C and 5% CO_2 under a constant flow of supplemented medium for one night at 0.6 μL/min and then maintained at 1μL/min for typically four days. The latter flow rate corresponds to a wall shear stress of ∼0.4 Pa, representative of physiological conditions in *e.g.* post-capillary venules[32]. In order to assess the response of such shear-adapted cells to a decrease in wall shear stress, the flow was reduced from 0.4 to 0.08 Pa for 1 or 6 hours, after which cells were fixed as described below. As a control, HUVEC were also cultured under static condition into fibronectin-coated glass-bottom Petri dishes until reaching confluence.

For confocal microscopy we used the following dyes: (i) Hoechst 33342 (Molecular Probes) for nuclei staining, (ii) Phalloidin TRITC (Sigma-Aldrich) for F-Actin staining and (iii) Wheat Germ Agglutinin (WGA) Alexa Fluor 488 Conjugate (5 μg/ml, Molecular Probes) for staining the glycocalyx. The dyes were used in accordance with manufacturer's specification. Staining were performed after fixation by flowing in the channels a solution of 4% paraformaldehyde in PBS for 30 min at 37 °C.

For glycocalyx modification, cells were exposed to Neuraminidase from Clostridium perfringens (1U/ml, Sigma-Aldrich) for 60 min in a CO_2 incubator. Neuraminidase was used at 150 mUI/mL for 3 hours in non-supplemented endothelial cells culture medium. Glycocalyx was stained by WGA-Alexa 488 after enzymatic modification and fluorescence intensity was estimated with and without Neuraminidase action.

C. Imaging and analysis

Confocal fluorescence microscopy was performed on an inverted microscope. XYZ image stacks were obtained in raster mode using a Zeiss LSM710 module and a 40×/NA1.3 oil-immersion objective, with a lateral size of 1024×200 pixels, a lateral resolution of 0.225 μm/pixel, and a Z-slice spacing of 0.46 μm.

The acquired image stacks were processed and analyzed using the Fiji open-source platform and its built-in plugins. 3-dimensional XYZ image stacks were treated as follows. A point spread function (PSF) of the microscope was generated numerically with Fiji, using the "Diffraction PSF 3D" plugin fed with the experimental characteristics of our imaging system (i.e. refraction index of immersion liquid, objective numerical aperture, lateral magnification and z slice spacing of the stack). We have further checked for the consistency of such a generated PSF by using it to deconvolve images of fluorescent latex beads of known diameter (500 nm) and ensuring that the bead size measured from the deconvolved images agreed with the expected one. PSF deconvolution was then performed on image stacks of the stained cells using the "Iterative deconvolve 3D" plugin. Z-projection of deconvolved image stacks were then made, summing the intensity of each of the slices spanning the EC monolayer adhered on the bottom surface of the channels.

From such Z-projections, F-Actin structures were characterized with the Fiji plugin "OrientationJ", using the "Gaussian gradient" built-in method with a window size of 2 pixels (see Results section for details). Such an analysis was performed, for each culture condition, on images taken from the 16 central microchannels of the devices, over duplicate or triplicate experiments. Total numbers of analyzed cells were: $N = 389$ for culture under flow at 0.4 Pa, $N = 235$ for flow reduced at 0.08 Pa for 1h, $N = 311$ for flow reduced at 0.08 Pa for 6h, $N = 143$ for neuraminidase treatment, and $N = 132$ cells under static condition.

III. RESULTS

A. Flow *vs* static condition and quantification of filamentous actin structures

As reported previously[31], and as illustrated on Fig. 1B, HUVEC cultured under flow for several days yield a monolayer of cells covering the four walls of the microchannels. Under such conditions, we observe that cells exhibit many oriented actin stress fibers that cross the cell from side to side underneath the nucleus and seem to be attached to cell-cell junction as they continue end to end into the neighboring cell (see Fig. 1C and D). In contrast to this, HUVEC cultured under static conditions rather display a marked deep peripheral actin band, with no or few randomly oriented stress fibers (Fig. 1E).

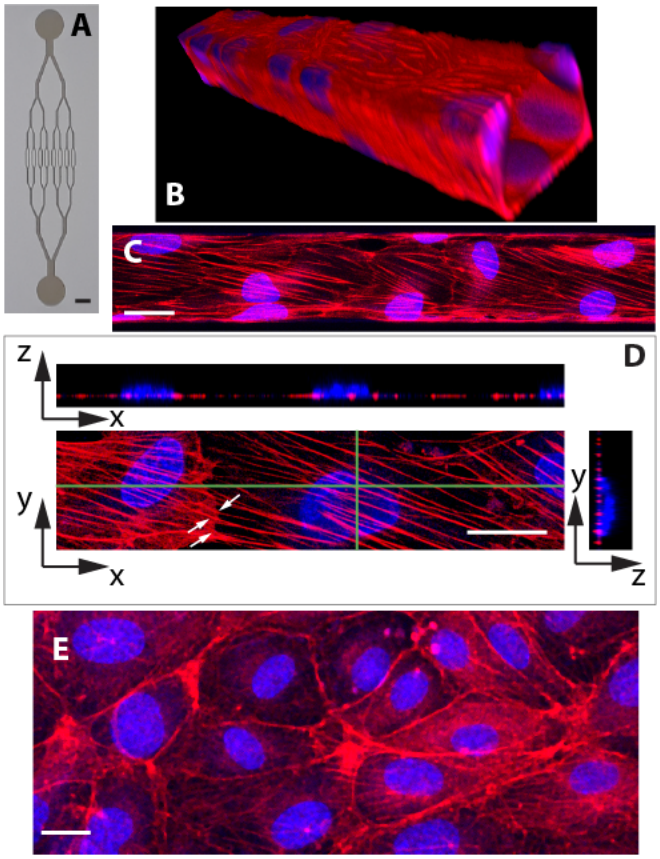

FIG. 1. (A) Picture of the resin mold showing the geometry of the microfluidic network (scale bar : 1 mm). (B) 3D rendering of images from a portion of channel covered by HUVEC, having a cross-section of $30 \times 30\,\mu\text{m}^2$ and a length of 212 μm (overlay of F-actin (red) and nuclei (blue)). (C) Image of the bottom surface of a microchannel ($30 \times 30\,\mu\text{m}^2$ in cross-section), showing the thick and oriented actin fibers displayed by HUVEC cultured under 0.4 Pa (flow direction from left to right. Scale bar 20 μm). (D) Image of adjacent cells (xy panel) showing actin fibers "crossing" the the cells' boundary (white arrows). Stress fibers are located at the basal side of the cells, as seen on the two orthogonal images showing fiber cross-sections running below the nuclei (xz and yz panels taken along the directions indicated by green lines on the xy view. Scale bar 20 μm) (E) Image of HUVEC cultured under static conditions, showing F-actin being mainly localized at the periphery of the cells, with only few and randomly oriented fibers (scale bar 20 μm).

In order to quantify further the organization of filamentous actin, we use the features of the OrientationJ plugin[33] written for ImageJ. This plugin computes the structure tensor from the intensity gradient of an image, and attributes to each pixel in the image a pair of values, between 0 and 1, corresponding to the local values of the (normalized) energy, E, and coherency, C, of the structure tensor. Low values of E correspond to regions in the image where intensity is uniform, while large values indicate regions having one or multiple orientations. C is a measure of the local degree of anisotropy, with values closer to 1 corresponding to regions of stronger anisotropy. For each experimental conditions, we compute E and C maps of the F-actin images obtained (Fig. 2), and build a final map where each pixel contains the value of $\sqrt{EC}$. Plotting the distribution of $\sqrt{EC}$ allows us assessing, for a given cell culture condition, the fraction of image pixels involved in non-uniform and strongly elongated F-actin structures.

From the computation of the structure tensor, OrientationJ also provides a map of the local orientation. The plugin associates an orientation to each pixel in the image, including in regions of low E and C where this quantity is not meaningful. Such an orientation map can then be filtered by thresholding on E and C values in order to retain only the orientation values of pixels that are actually part of anisotropic structures. Doing so using the built-in thresholding feature of OrientationJ, we observe that, with our type of images, the filtered orientation maps display a spatial resolution that is clearly lower than the initial image, with blurred features and inclusion of pixels that are actually outside of the fibers (see Fig. 2). We could not find a set of OrientationJ parameters that would allow us to increase further the resolution of the orientation map without losing part of the elongated structures that are visible in the original image. As an alternative to the built-in thresholding feature of the plugin, we find that the following procedure performs better in terms of final resolution: starting from the input image, we run orientationJ to obtain E, C and unfiltered orientation maps. We then threshold the E and C images (at the same levels used in the built-in function of the plugin, namely $C > 0.6$ and $E > 0.1$ in the present work) and binarize them. In parallel, we binarize the input image using the local threshold Bernsen method implemented in ImageJ. We then multiply the binarized E, C and Bernsen image in order to create a binary mask that we use to filter the orientation map. A comparison of the built-in and custom-made thresholding is provided in Fig. 2. The orientation maps thus produced are then used to compute angular distributions. In the following, angular distributions are computed over 180 bins of width 1°, spanning the range between -90° and +90°, with 0° being the flow direction.

Applying the above-described procedure to F-actin images obtained under static and 0.4 Pa shear flow conditions, we observe that: (i) the distribution of $\sqrt{EC}$ is more populated towards large values ($\sqrt{EC} \geq 0.2$) for shear-adapted cells than for static condition (Fig. 3A), consistent with more anisotropic structures (*i.e.* stress fibers) being present in cells cultured under fflow, and (ii) the angular distribution of such structures is sharply peaked about 0° (*i.e.* along the flow direction) for shear-adapted cells (Fig. 3B), indicating streamwise alignment of stress fibers.

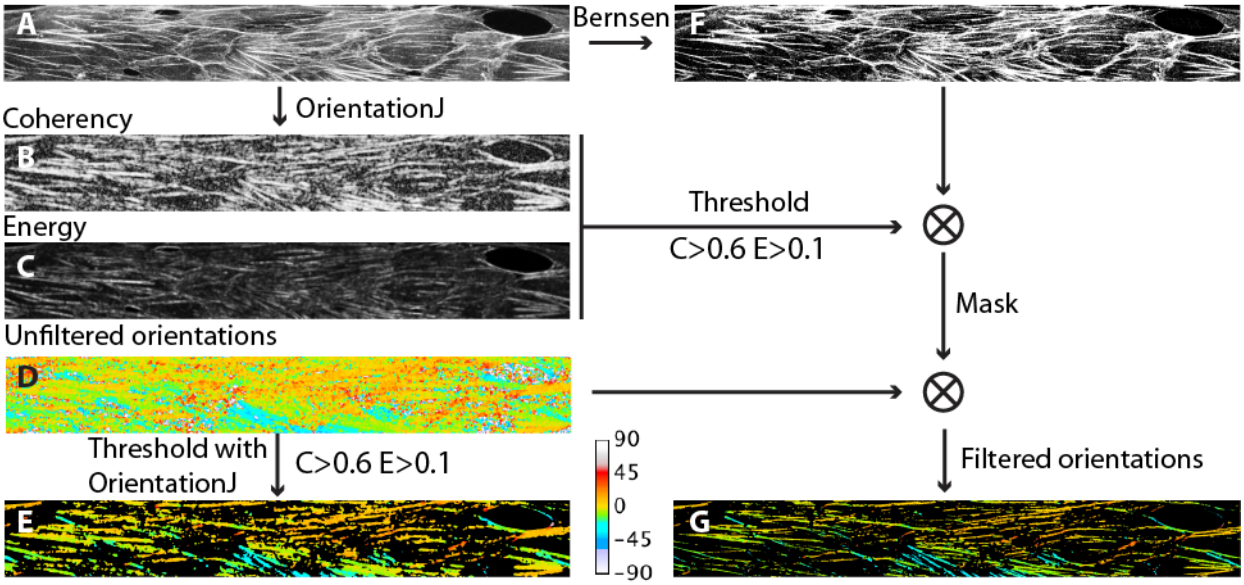

FIG. 2. Flowchart of image analysis: starting from a F-actin image (a), the OrientationJ plugin outputs Coherency (b), Energy (c), and Orientation (d) maps. OrientationJ allows filtering the orientation map in order to retain only pixels involved in regions having coherency and energy values larger than a given threshold ($E > 0.1$ and $C > 0.6$ here) (e). As an alternative to the latter step, we apply a local thresholding scheme (Bernsen) to the initial image (f) and multiply this segmented image by the thresholded maps (b) and (c) in order to create a binary mask. We then use such a mask in order to discard irrelevant pixels from the raw orientation map (d), and obtain the orientation map (g), with better spatial resolution than (e). Colors on images (d), (e) and (g) code for the local angle, according to the lookup table displayed at the bottom of the figure.

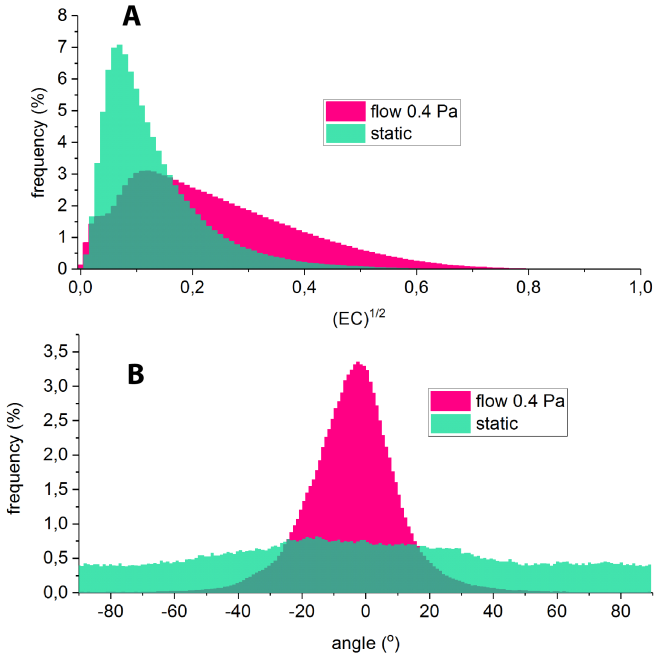

FIG. 3. (A) Distribution of $\sqrt{EC}$ for HUVEC cultured under 0.4 Pa in microfluidic channels (Magenta) and under static conditions (Green). (B) Angular distribution of actin filamentous structures observed under flow (Magenta) and static conditions (Green).

B. Effect of shear stress reduction and neuraminidase treatment

The effect of reducing the shear stress is illustrated on Fig. 4. Starting from cells adapted under 0.4 Pa, exhibiting numerous long and oriented stress fibers (Fig. 4A), we observe that a reduction of stress down to 0.08 Pa for 1h leads to a marked decrease in the number of fibers and to a localization of F-actin at the periphery of the cells (Fig. 4B). Such a trend is maintained after 6h of reduced flow (Fig. 4C). We also notice a slight increase in the thickness of the cells' nuclei under reduced flow conditions, as shown on Fig. 4D. In addition to this, we notice qualitatively that upon long exposure to low shear stress (6h or more), HUVEC tend to detach from the microchannel walls, mainly from the corners, as illustrated on Fig. 4E, while maintaining cell-cell contacts.

The decrease in the number of filamentous structures under 0.08 Pa can be seen on the distributions of $\sqrt{EC}$ computed for reduced shear conditions (Fig. 6A), which, as observed under purely static condition, peak at low values ($\sqrt{EC} < 0.2$) compared to that obtained for the 0.4 Pa flow condition. Such a loss of actin fibers under 0.08 Pa of wall shear stress is also accompanied by a broadening of the angular distributions, which exhibit tails beyond $\pm 40°$ that are more pronounced than at 0.4 Pa (Fig. 6B). While our image analysis procedure does not allow us to discriminate between the various contributions, the observed angular broadening under reduced

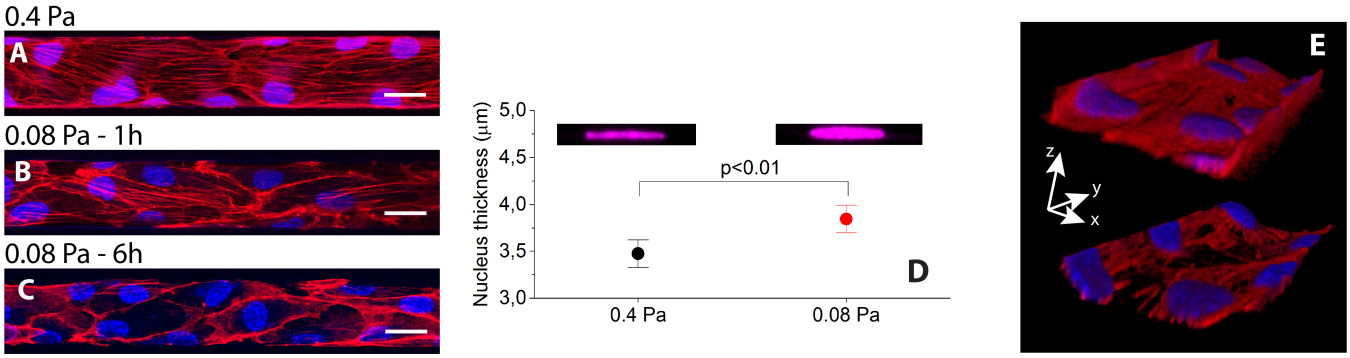

FIG. 4. Overlay images of cells' nuclei (blue) and F-actin (red) under 0.4 Pa (A), 1h at 0.08 Pa (B) and 6h at 0.08 Pa (C). Panel (D): Vertical projections of nucleus under 0.4 Pa (left image) and 0.08 Pa (right image). Such images were taken over about 80 cells for each condition (0.4 Pa and 6h at 0.08 Pa) and used to measure the maximum thickness of the nuclei. The plot reports the mean of these measurements (error bars correspond to 99% confidence interval), which is seen to be $\sim 0.3\,\mu$m larger ($p < 0.01$ in two-sample t-test) under low shear condition. (E) 3D reconstructions of the bottom part of a channel showing cells lying in the corners under 0.4 Pa (top image), while they tend to detach from corners and round up the effective lumen under 0.08 Pa (bottom image). The lateral channel size is 30 μm.

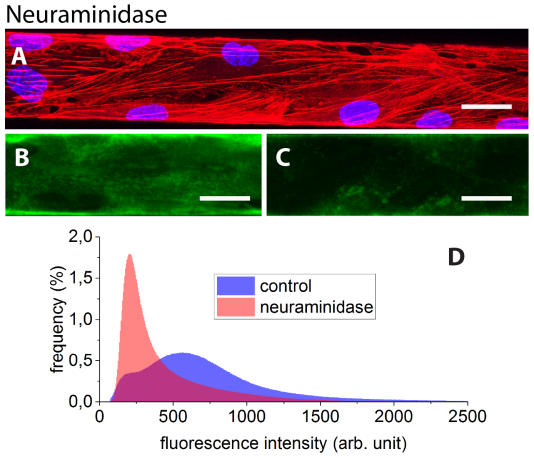

FIG. 5. (A) Nuclei and F-actin image of cells after neuraminidase treatment. WGA-Alexa fluorescence images taken before (B) and after (C) treatment show a marked decrease in intensity upon treatment, as confirmed by fluorescence intensity histograms (D).

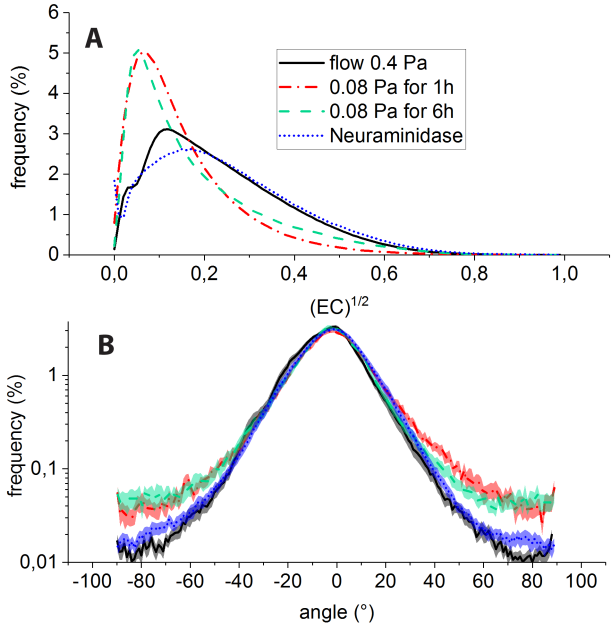

FIG. 6. (A) Distributions of $\sqrt{EC}$ computed for the various conditions indicated in the panel legend. (B) Angular distributions obtained for the various flow and treatment conditions. Color code as in (A). Each distribution is plotted as mean ± standard error (thick line ± shaded area) computed from the analysis of $\sim$ 30 different fields of view for each condition.

flow can stem from both a disorientation of stress fibers and from the buildup of peripheral actin, both contributing to large angles in the distributions.

Finally, we note that the degradation of the glycocalyx using neuraminidase, resulting in a clear decrease of the WGA-Alexa fluorescence signal (see Fig. 5) which indicates actual removal of some components of the ESL, does not induce any clear change of the F-actin organization: we observe cells displaying numerous and flow oriented stress fibers (Fig. 5A) yielding distributions of $\sqrt{EC}$ and angles very similar to that of intact and flow adapted cells (Fig. 6).

IV. DISCUSSION AND CONCLUSION

The partial degradation of the ESL with neuraminidase yielding no discernible change in actin organization may seem puzzling in the first place, as the glycocalyx is directly involved in flow sensing of endothelial cells. However, neuraminidase specifically

targets syalic acid in the ESL, while it is expected to leave intact glycosaminoglycans such as Heparan Sulfate[34]. Our observation is therefore qualitatively consistent with previous studies pointing at heparan sulfate as being one of the main player, connected to the cyctoskeleton through syndecans, in glycocalyx-mediated mechanotransduction[7,8,13,35,36].

Furthermore, our experiments indicate that HUVEC cultured under a steady shear flow corresponding to a wall stress of 0.4 Pa display long and flow-oriented F-actin fibers. This observation is consistent with previous works and shows that the well-established picture of the atheroprotective phenotype holds in a situation where the endothelial cells are strongly confined and organized in 3D into capillary-sized microchannels. Our study demonstrates that, starting from such a phenotype, HUVEC respond within one hour to a lowering of wall shear stress down to 0.08 Pa by a marked rearrangement of the actin cytoskeleton, with stress fibers being disrupted/disorganized and actin being redistributed into the cells' peripheral band. The concomitantly observed thickening of the nuclei, which suggests a slight inflation of the cells' body, is consistent with a decrease in the number of stress fibers, which we expect to be associated with a relaxation of the cells' internal stresses.

This set of results, along with the trend for cells to detach from the walls at long exposure to low shear, strongly suggests that upon a five-fold decrease of the wall shear stress, HUVEC switch from an atheroprotective to an atheroprone and more motile phenotype[37]. While previous studies have highlighted differences in phenotypes in response to flow start-up[9] or to various flow patterns applied from the start of the culture[1,22,37], the present study is, to the best of our knowledge, the first to report on cytoskeleton reorganization of shear-adapted cells in response to a flow decrease. We note that such a response involves a reorganization of the actin skeleton that shares features (disruption of fibers, actin buildup at cells' periphery) with what has been observed as a result of exposing endothelial cells to simulated microgravity[38]. This suggests that, in the context of vascular adaptation to space flight conditions, both microgravity and altered blood flow act in concert to induce phenotypic changes of endothelial cells.

ACKNOWLEDGMENTS

We acknowledge the department of Material Sciences of the french Centre National d'Etudes Spatiales (CNES) for financial support. M.I is a PhD fellow of the France-Germany "Living fluids" Doctoral school.

[1] J.-J. Chiu and S. Chien, Physiol. Rev. **91**, 327 (2011).
[2] P. F. Davies, Nat Rev Cardiol **6**, 16 (2008).
[3] S. Chien, AJP: Heart and Circulatory Physiology **292**, H1209 (2007).
[4] M. J. Levesque and R. M. Nerem, J Biomech Eng **107**, 341 (1985).
[5] O. Traub and B. C. Berk, Arteriosclerosis, Thrombosis, and Vascular Biology **18**, 677 (1998).
[6] S. Reitsma, D. W. Slaaf, H. Vink, M. A. M. J. van Zandvoort, and M. G. A. oude Egbrink, Pflugers Arch - Eur J Physiol **454**, 345 (2007).
[7] J. A. Florian, J. R. Kosky, K. Ainslie, Z. Pang, R. O. Dull, and J. M. Tarbell, Circulation Research **93**, H1145 (2003).
[8] M. M. Thi, J. M. Tarbell, S. Weinbaum, and D. C. Spray, Proc Natl Acad Sci USA **101**, 16483 (2004).
[9] Y. Zeng and J. M. Tarbell, PLoS ONE **9**, e86249 (2014).
[10] P. F. Davies, Physiol. Rev. **75**, 519 (1995).
[11] E. Tzima, M. Irani-Tehrani, W. B. Kiosses, E. Dejana, D. A. Schultz, B. Engelhardt, G. Cao, H. DeLisser, and M. A. Schwartz, Nature **437**, 426 (2005).
[12] V. Rizzo, C. Morton, N. DePaola, J. E. Schnitzer, and P. F. Davies, AJP: Heart and Circulatory Physiology **285**, H1720 (2003).
[13] J. M. Tarbell and M. Y. Pahakis, J Intern Med **259**, 339 (2006).
[14] S. Noria, D. B. Cowan, A. I. Gotlieb, and B. L. Langille, Circulation Research **85**, 504 (1999).
[15] S. Noria, F. Xu, S. McCue, M. Jones, A. I. Gotlieb, and B. L. Langille, The American Journal of Pathology **164**, 1211 (2010).
[16] R. P. Franke, M. Gräfe, H. Schnittler, D. Seiffge, C. Mittermayer, and D. Drenckhahn, Nature **307**, 648 (1984).
[17] C. G. Galbraith, R. Skalak, and S. Chien, Cell Motil. Cytoskeleton **40**, 317 (1998).
[18] A. J. Wong, T. D. Pollard, and I. M. Herman, Science **219**, 867 (1983).
[19] V. Nehls and D. Drenckhahn, Microvascular Research **42**, 103 (1991).
[20] B. L. Langille, J. J. Graham, D. Kim, and A. I. Gotlieb, Arterioscler. Thromb. **11**, 1814 (1991).
[21] A. D. van der Meer, A. A. Poot, J. Feijen, and I. Vermes, Biomicrofluidics **4**, 011103 (2010).
[22] C. Zheng, X. Zhang, C. Li, Y. Pang, and Y. Huang, Anal. Chem. **89**, 3710 (2017).
[23] F. Tovar-Lopez, P. Thurgood, C. Gilliam, N. Nguyen, E. Pirogova, K. Khoshmanesh, and S. Baratchi, Front. Bioeng. Biotechnol. **7**, pe6 (2019).
[24] A. B. Fisher, S. Chien, A. I. Barakat, and R. M. Nerem, AJP: Lung Cellular and Molecular Physiology **281**, L529 (2001).
[25] Y. Manevich, A. Al-Mehdi, V. Muzykantov, and A. B. Fisher, AJP: Heart and Circulatory Physiology **280**, H2126 (2001).
[26] J. R. Leemreis, A. M. G. Versteilen, P. Sipkema, A. B. J. Groeneveld, and R. J. P. Musters, Cytometry **69A**, 973 (2006).
[27] T. Milovanova, S. Chatterjee, B. J. Hawkins, N. Hong, E. M. Sorokina, K. DeBolt, J. S. Moore, M. Madesh, and A. B. Fisher, Biochimica et Biophysica Acta (BBA) - Molecular Cell Research **1783**, 1866 (2008).
[28] L. F. Zhang, Journal of Applied Physiology **91**, 2415 (2001).
[29] R. L. Hughson, A. Helm, and M. Durante, Nat Rev Cardiol **15**, 167 (2018).
[30] M. D. Delp, P. N. Colleran, M. K. Wilkerson, M. R. McCurdy, and J. Muller-Delp, AJP: Heart and Circulatory Physiology **278**, H1866 (2000).
[31] D. Tsvirkun, A. Grichine, A. Duperray, C. Misbah, and L. Bureau, Sci. Rep. **7**, 45036 (2017).
[32] S. Sheikh, G. E. Rainger, Z. Gale, M. Rahman, and G. B. Nash, Blood **102**, 2828 (2003).
[33] R. Rezakhaniha, A. Agianniotis, J. T. C. Schrauwen, A. Griffa, D. Sage, C. V. C. Bouten, F. N. van de Vosse, M. Unser, and N. Stergiopulos, Biomech Model Mechanobiol **11**, 461 (2011).
[34] M. Y. Pahakis, J. R. Kosky, R. O. Dull, and J. M. Tarbell, Biochem. Biophys. Res. Commun. **355**, 228 (2007).
[35] E. E. Ebong, S. V. Lopez-Quintero, V. Rizzo, D. C. Spray, and J. M. Tarbell, Integr. Biol. **6**, 338 (2014).
[36] W. Yen, B. Cai, J. Yang, L. Zhang, M. Zeng, J. M. Tarbell, and B. M. Fu, PLoS ONE **10**, e0117133 (2015).
[37] G. Dai, M. R. Kaazempur-Mofrad, S. Natarajan, Y. Zhang, S. Vaughn, B. R. Blackman, R. D. Kamm, G. García-Cardeña,

and M. A. Gimbrone, Proc Natl Acad Sci USA **101**, 14871 (2004).
[38]S. Versari, A. Villa, S. Bradamante, and J. A. M. Maier, Biochimica et Biophysica Acta (BBA) - Molecular Cell Research **1773**, 1645 (2007).